

Novel Impregnation–Deposition Method to Synthesize a Presulfided $\text{MoS}_2/\text{Al}_2\text{O}_3$ Catalyst and Its Application in Hydrodesulfurization

Xuehui Li,^{*,†} Xuefeng Wang,[†] Jing Ning, Hongtao Wei, and Long Hao^{*}Cite This: *ACS Omega* 2023, 8, 2596–2606

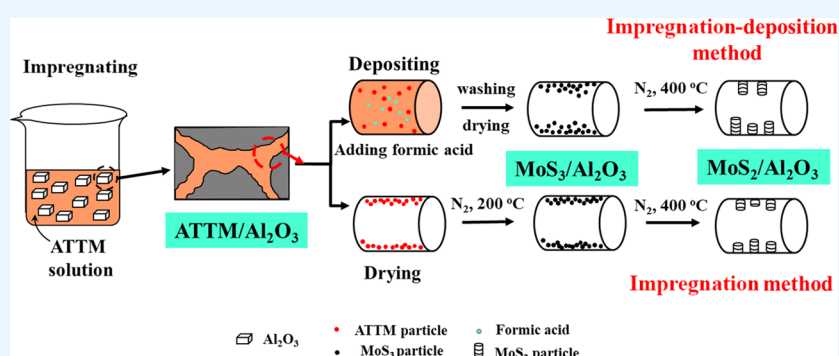
Read Online

ACCESS |

Metrics & More

Article Recommendations

Supporting Information



ABSTRACT: A novel impregnation–deposition method was applied to prepare presulfided $\text{MoS}_2/\text{Al}_2\text{O}_3$ catalysts with large surface areas for the application of hydrodesulfurization (HDS). The synthesized catalysts were characterized systematically, and their catalytic performances were evaluated by the HDS of dibenzothiophene (DBT). It is found that the impregnation–deposition method improves the surface area of the synthesized catalysts by eliminating the micropores of the alumina support and adding mesostructured MoS_2 particles within the support. Moreover, this method enhances the reducibility of the sulfided Mo species, as characterized by temperature-programmed reduction (TPR) and X-ray photoelectron spectroscopy. Compared to the impregnation method, the impregnation–deposition method leads to the formation of more active sites as proved by TPR and CO-Fourier-transform infrared analyses. Hence, the reaction conversion rates and the hydrogenation/direct-desulfurization ratios of the DBT on the catalysts synthesized by the impregnation–deposition method are 1.3 times and 1.5 times as high as those of the catalysts made by the conventional impregnation method, respectively.

1. INTRODUCTION

Increasing attention is being paid to the fuel processing industries all over the world. Under the pressure of the lower-quality crude oil and the increasingly rigorous environmental problems, the sulfur content in fuels has been limited to an extremely low level (<10 ppm).^{1,2} Up until now, as one of the important techniques to produce ultra-clean fuels, the hydrodesulfurization (HDS) technology might be the most effective approach to remove the sulfur-containing compounds in refining industries.^{3–6}

In order to meet the strict regulations,^{7,8} transition metal compounds, such as transition metal sulfides/phosphides, etc., have been widely used as catalysts for ultraclean fuel production.^{9–12} Generally, Co/Ni-promoted MoS_2 catalysts supported on Al_2O_3 are the most commonly applied catalysts in HDS processes.¹³ Two types of active phases are usually contained in the catalysts: the lower active type I phase interacting strongly with the Al_2O_3 support via Mo–O–Al bonds and the higher active type II phase interacting weakly with Al_2O_3 by the van der Waals force.¹⁴ The conventional

Mo-based HDS catalysts are usually prepared by the sulfidation of $\text{MoO}_x/\text{Al}_2\text{O}_3$. However, a great number of Mo–O–Al linkages are formed during the preparation of $\text{MoO}_x/\text{Al}_2\text{O}_3$, which will cause the subsequent insufficient sulfidation and the formation of majority type I active sites. All of these will finally lead to the decrease in the catalytic activity of $\text{MoS}_2/\text{Al}_2\text{O}_3$. Consequently, improving the sulfidation degree and creating more type II active sites are very important.

Recently, ammonium tetrathiomolybdate [ATTM, $(\text{NH}_4)_2\text{MoS}_4$] has attracted significant attention as an established active component for the preparation of catalysts in the sulfuric form (i.e., the presulfided catalysts).^{11,15,16} It was

Received: November 4, 2022

Accepted: December 30, 2022

Published: January 9, 2023



found that the molybdenum sulfide catalyst prepared by the decomposition of ATTM exhibited a good activity toward thiophene hydrogenolysis.^{17,18} Catalytic hydrogenolysis activity was directly correlated with the number of anion vacancies and the low valence state of the reduced $\text{MoS}_2/\text{Al}_2\text{O}_3$ catalysts. Moreover, as ATTM has already tetrahedrally bonded to molybdenum atoms, which simplifies the sulfidation of oxide precursors,¹⁹ the decomposition of ATTM will lead to completely sulfided catalysts.

Up until now, the impregnation method has been widely used for the preparation of conventional HDS catalysts due to the simple and economical operations.²⁰ Many studies have been conducted on supported catalysts prepared from the ATTM precursor.^{19,21,22} A series of highly loaded $\text{MoS}_2/\text{Al}_2\text{O}_3$ HDS catalysts were prepared by impregnating and reducing ATTM with N_2H_4 in aqueous solution in the presence of Al_2O_3 .²³ The catalyst activity increased until the Mo content was up to 22 wt %, in contrast to those conventional oxide precursor routes, for which the catalytic activity stabilized after the Mo content was more than 15 wt %.²⁴ Although ATTM is an excellent active component for HDS catalysts, the preparation methods are still unsatisfactory because these catalysts have highly decreased surface areas due to the blocked pore structures caused by aggregated active components. Therefore, taking advantage of the excellent properties of ATTM and optimizing the pore structures of the catalysts are a key point to improve the catalytic activity.

The deposition method is an optimal procedure to synthesize unsupported MoS_2 catalysts with high specific areas and excellent activities due to the ease of preparation and homogeneity of the as-prepared catalysts.^{25–29} Moreover, several approaches have been proposed in the supported catalyst preparation based on this method, such as the chemical deposition method,³⁰ the in situ deposition method,³¹ the chemical vapor deposition method,³² and the pulsed laser deposition method.²⁷ Shi et al. reported a simple ethanol-assisted chemical deposition method to synthesize a $\text{MoS}_2/\text{Al}_2\text{O}_3$ catalyst with a large specific surface area and high sulfidation degree of Mo species.³³ A similar method was also employed by Gao et al. in the preparation of HDS catalysts using MoS_3 nanoparticles as the precursor.³⁴ They found that the as-synthesized MoS_3 precursor not only promoted the sulfidation degree of the resulting catalyst but also realized a superior decoration of Ni atoms at the edges of MoS_2 nanoflakes. The MoS_2 active phases in the reported catalysts, however, are still generated by an ex situ sulfidation and thermal treatment process with the oxidic Mo species, which will lead to an insufficient utilization of Mo species.

The combination of impregnation and deposition is an effective way to synthesize catalysts with ideal porous structures and excellent catalytic performances. Nevertheless, to the best of our knowledge, this method has still not been applied in the presulfided HDS catalyst preparation. This work aims to develop a simple and convenient method to synthesize a presulfided HDS catalyst with superior catalytic behavior. For this target, ATTM was selected as the precursor due to its high sulfidation degree and excellent HDS activity. In the meantime, the impregnation–deposition method was also selected to optimize the structural and catalytic properties of the catalysts. The textural properties of the catalysts and the dispersity of the active components were characterized. The catalytic activity of $\text{MoS}_2/\text{Al}_2\text{O}_3$ catalysts synthesized by the impregnation–deposition method was investigated.

2. EXPERIMENTAL SECTION

2.1. Catalyst Preparation. All of the chemicals were purchased from Sinopharm Chemical Reagent Company (PR China) without further purification. The cylindrical extrudates of the Al_2O_3 support (with a diameter of 1.2 mm and an average length of 3 mm) were prepared using a twin-screw extruder at a revolving speed of 300 rpm. Before extrusion, nitric acid (1.0 g), deionized water (70 mL), and sesbania powder (1.0 g) were added to pseudo-boehmite (100 g) and stirred well. Then, the extrudates were dried at 120 °C for 10 h and calcined at 550 °C for 4 h.

ATTM was prepared according to the method described by Alonso et al.³⁵ Generally, ammonium heptamolybdate [$(\text{NH}_4)_6\text{Mo}_7\text{O}_{24}\cdot 4\text{H}_2\text{O}$, 4.8 g] was first dissolved in ammonium hydroxide (50 mL) and purged with hydrogen sulfide (H_2S) for sulfidation at room temperature for 1 h. Then, the mixture was heated to 60 °C with the continuous H_2S purging until a deep-red color appeared. After this, the mixture was cooled in an ice bath for 12 h for the crystallization of ATTM. Finally, the ATTM crystals could be obtained after the vacuum filtration, washed five times with cold ethyl alcohol, and dried under vacuum.

The synthesized ATTM was dispersed on the Al_2O_3 support by the incipient wetness impregnation method. The impregnation solution was prepared by adding 3.0 g of ATTM and 1.5 g of ethanolamine in 9.0 mL of deionized water. Afterward, the solution was mixed with 10 mL of Al_2O_3 extrudates and placed at room temperature for 12 h. For the conventional impregnation method, the impregnated materials were dried in N_2 at 120 °C for 12 h and calcined at 400 °C for 4 h with a 4 °C/min heating ramp. Active phase molybdenum (Mo) was prepared in a ratio of 20 % wt. The corresponding presulfided $\text{MoS}_2/\text{Al}_2\text{O}_3$ catalyst was labeled $\text{MoS}_2\text{-I}/\text{Al}_2\text{O}_3$. For the impregnation–deposition method, the same impregnating process was utilized, and the impregnated materials were added to a formic acid solution [0.92 g of formic acid (99%) added in 20 mL of deionized water] at room temperature for 1 h to guarantee a complete deposition. Then, the materials were filtered and washed several times with deionized water. After this, the as-synthesized materials were calcined in N_2 at 400 °C for 4 h with a 4 °C/min heating ramp. Active phase molybdenum (Mo) was also prepared in a ratio of 20 % wt, and the corresponding catalyst was labeled $\text{MoS}_2\text{-ID}/\text{Al}_2\text{O}_3$.

2.2. Characterization. A description in detail about all techniques has been supplied elsewhere,³⁶ and only a brief summary is provided here. The X-ray diffraction (XRD) patterns of the support and catalysts were recorded using a Panalytical X'Pert Pro MPD diffractometer (Netherlands, radiation $\text{Cu K}\alpha$, accelerating voltage 40 kV, applied current 30 mA, scan rate 0.05° s^{-1}).

Nitrogen adsorption–desorption isotherms were measured on a Micromeritics TRISTAR 3020 adsorption analyzer (USA). N_2 was used as the adsorption agent at –196 °C. Before the adsorption measurements, the samples should be degassed at 140 °C under a vacuum of 10^{-5} Torr for 5 h. The surface areas were calculated according to the Brunauer–Emmett–Teller (BET) method. The pore size distributions were obtained from the branch of the isotherms in the Barrett–Joyner–Halenda (BJH) method.

The properties of surface sites were determined by Fourier-transform infrared (FT-IR) measurements after the adsorption of CO at low temperature (100 K). A Bruker VERTEX 70

digital FT-IR spectrometer equipped with a CO adsorption system has been used. For the CO-FTIR study, samples were carefully ground and placed into the IR cell. The samples were first dried in situ at 300 °C under normal pressure in N₂ for 2 h. Then, they were cooled to 30 °C and treated with H₂ at a heating rate of 10 °C/min to 300 °C for 2 h. Afterward, the sample was cooled to 100 K with liquid nitrogen under high vacuum (1 × 10⁻⁴ Pa), and the background was obtained under this condition. Small doses of CO were introduced by a calibrated volume at an equilibrium pressure of 133 Pa to obtain site saturation. The IR spectra of adsorbed CO were recorded using a mercury–cadmium–telluride detector with 4 cm⁻¹ resolution and 256 scans.

The temperature-programmed reduction (TPR) measurements were carried out with a Quantachrome CHEMBET-3000 instrument. Before the measurements, the samples (0.1 g) were first charged in a loop and heated to 180 °C at a rate of 10 °C/min and maintained for 1 h under Ar flow to remove the adsorbed materials. Then, the samples were cooled to room temperature and treated in H₂/Ar (10 vol %) with a flow rate of 100 mL min⁻¹ at room temperature for 1 h. After this, the samples were heated from 50 to 800 °C at a rate of 10 °C min⁻¹. In the process, a thermal conductivity detector was used to measure the consumption of hydrogen.

X-ray photoelectron spectroscopy (XPS) analyses were performed on a VG ESCALAMBK II spectrometer equipped with a multi-channel detector and non-monochromatic Al K alpha radiation (1486.6 eV) with an excitation power of 15 kW and 10 mA. The analytic chamber vacuum prior to the test was 5.0 × 10⁻⁹ mbar. Before analyses, the sulfided catalysts were placed in a box under Ar to avoid the partial reoxidation. The samples were pressed onto the specimen holder, which was directly moved into the introduction chamber. All the bonding energies were determined by using C 1s (284.6 eV) as the reference. The Mo 3d, S 2p, and Al 2p spectra were analyzed with a XPSPEAK V4.1 software package. The Shirley background was subtracted from the data, and a Gaussian–Lorentzian decomposition with a 20/80 proportion was applied as the parameter. The binding energy values were estimated to be accurate within ±0.2 eV.

Transmission electron microscopy (TEM) was performed with a JEM-2100UHR electron microscope (JEOL, Japan), and the accelerating voltage was 200 kV. The catalysts were ground and suspended in ethanol using an ultrasonic bath and then placed in a Cu cellulose-coated grille. About 300 slabs from nearly 15 representative micrographs were taken to quantitatively compare the average length and stacking number of the MoS₂ slabs on different catalysts, and the statistically calculated formulas are listed as eqs 1–4.^{11,37,38}

$$\bar{L} = \frac{\sum_{i=1}^n n_i L_i}{\sum_{i=1}^n n_i} \quad (1)$$

$$\bar{N} = \frac{\sum_{i=1}^n n_i N_i}{\sum_{i=1}^n n_i} \quad (2)$$

where n_i is the number of MoS₂ units, L_i is the length of MoS₂ units, and N_i represents the layer number of stacked MoS₂ units.

$$n'_i = \frac{10 \times \bar{L} / 3.2 + 1}{2} \quad (3)$$

$$f_{\text{Mo}} = \frac{\sum_{i=1, \dots, t} 6n'_i - 6}{\sum_{i=1, \dots, t} 3n'_i{}^2 - 3n'_i + 1} \quad (4)$$

where n'_i is the number of Mo atoms along one side of the MoS₂ slabs and f_{Mo} is the proportion of Mo at the edge site.

2.3. Catalytic Activity Assessment. The catalytic activity measurements were carried out in a continuous-flow fixed-bed high-pressure micro-reactor (15 mm inner diameter and 650 mm long). Prior to the reaction, 4.2 g of catalysts (5 mL) was placed at the center of the reactor. Then, the catalysts were activated in hydrogen under a pressure of 2.0 MPa at 400 °C for 1 h (the heating rate of the reactor is 10 °C/min). After this, the temperature was reduced to 300 °C, and 2.0 wt % dibenzothiophene (DBT) in toluene was introduced into the reactor as the model reactant at a liquid hour space velocity of 2 h⁻¹ and a H₂/oil volumetric ratio of 300/1. The measurement was kept at 300 °C for 4 h, and the products were cooled and separated into gas and liquid products in a high-pressure separator behind the reactor. The liquid products were then collected using chromatographic sample bottles and analyzed on a Bruker 450 GC gas chromatograph equipped with a flame ionization detector and HP-5 capillary column.

The reaction rates of the presulfided MoS₂/Al₂O₃ catalysts toward DBT were calculated according to the equation³⁹

$$r_{\text{DBT}} = \frac{F}{m} \times \text{Conv}_{\text{DBT}} \quad (5)$$

where r_{DBT} is the reaction rate of DBT (mol/g·s), F is the molar flow rate of the reactant (mol/s), m is the weight of the presulfided MoS₂/Al₂O₃ catalyst (g), and Conv_{DBT} is the conversion of DBT.

3. RESULTS AND DISCUSSION

3.1. XRD Pattern Analyses. The XRD patterns of MoS₂ and the corresponding catalysts synthesized by different methods are listed in Figure 1. For unsupported MoS₂ particles MoS₂-ID, ATTM was deposited by formic acid and calcined at 400 °C in a N₂ atmosphere. As to MoS₂-I, ATTM

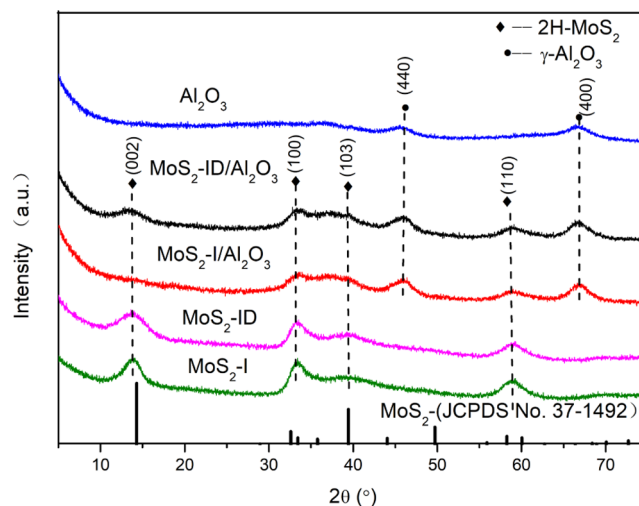


Figure 1. XRD patterns of the presulfided catalysts prepared by different methods MoS₂-ID/Al₂O₃, MoS₂-I/Al₂O₃, and the support Al₂O₃ and MoS₂ prepared by different methods MoS₂-ID and MoS₂-I and the JCPDS card no.37-1492.

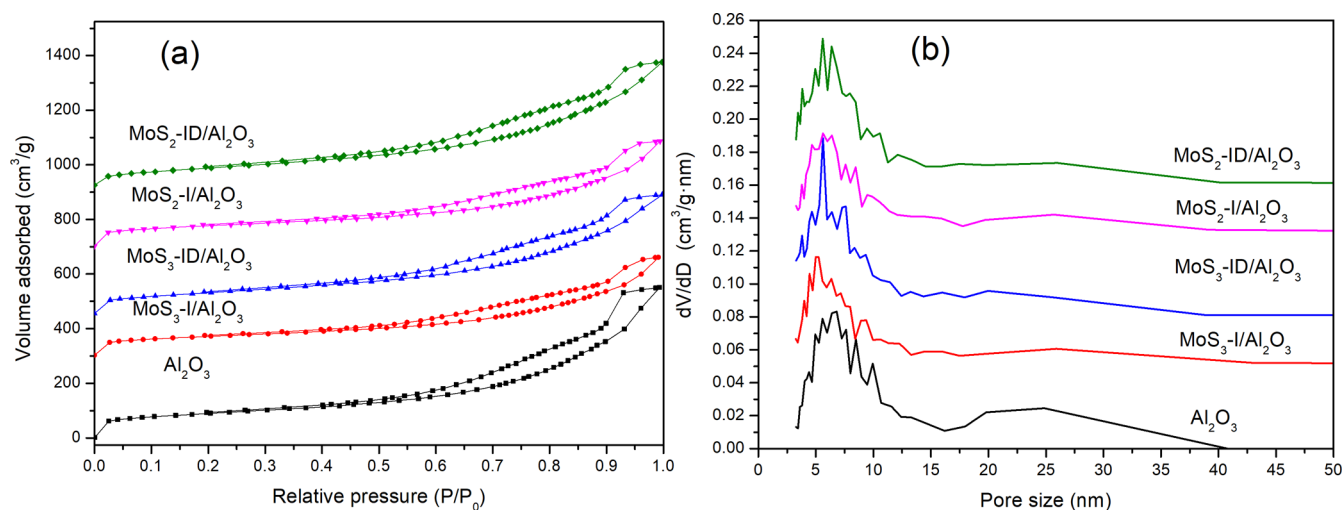


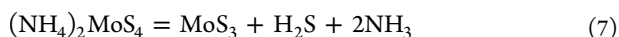
Figure 2. (a) N_2 adsorption isotherms and (b) pore size distributions of the presulfided catalysts $\text{MoS}_2\text{-ID}/\text{Al}_2\text{O}_3$ and $\text{MoS}_2\text{-I}/\text{Al}_2\text{O}_3$ and the precursor catalysts $\text{MoS}_3\text{-ID}/\text{Al}_2\text{O}_3$ and $\text{MoS}_3\text{-I}/\text{Al}_2\text{O}_3$ synthesized by different methods and the support Al_2O_3 .

was only calcined at 400 °C in N_2 . Both samples exhibit a good MoS_2 crystalline phase [14.1° (002), 33.2° (100), 39.3° (103), and 58.8° (110), JCPDS file no. 37-1492], and no significant difference exists in the peak intensity between them. When the MoS_2 active phase was supported on alumina by the impregnation and the impregnation–deposition methods, characteristic peaks ascribed to $\gamma\text{-Al}_2\text{O}_3$ [45.9° (440) and 66.8° (400)] and MoS_2 were observed in both samples. The crystallinities of the supported MoS_2 samples ($\text{MoS}_2\text{-ID}/\text{Al}_2\text{O}_3$ and $\text{MoS}_2\text{-I}/\text{Al}_2\text{O}_3$) were obviously lower than those of the unsupported MoS_2 samples ($\text{MoS}_2\text{-ID}$ and $\text{MoS}_2\text{-I}$), indicating that the MoS_2 crystals were well dispersed on the Al_2O_3 supports by both methods.⁹ The XRD patterns for the catalysts $\text{MoS}_2\text{-ID}/\text{Al}_2\text{O}_3$ and $\text{MoS}_2\text{-I}/\text{Al}_2\text{O}_3$ were also the same except for a broad diffraction peak at 14.1° in $\text{MoS}_2\text{-ID}/\text{Al}_2\text{O}_3$. This indicates that the crystallinity of MoS_2 on the supported catalysts could be affected by the preparation methods. It is known that the crystal structure of MoS_2 consists of a vertical arrangement of MoS_2 layers attached by van der Waals forces, and the (002) reflection peak comes from a certain stacking degree along the c direction.⁴⁰ Hence, the stacking degree of MoS_2 slabs prepared by the impregnation–deposition method is higher than that of MoS_2 slabs prepared by the impregnation method. The impregnation–deposition method is more favorable to generate MoS_2 crystals with a higher stacking degree.

3.2. Textural Properties. In this work, the precursor ATTM in both catalysts decomposed in the same form of $(\text{NH}_4)_2\text{MoS}_4 \rightarrow \text{MoS}_3 \rightarrow \text{MoS}_2$. For the catalyst $\text{MoS}_2\text{-ID}/\text{Al}_2\text{O}_3$ prepared by the impregnation–deposition method, ATTM was first impregnated in the Al_2O_3 support, and the as-synthesized wet sample was added to formic acid solution subsequently. The formic acid reacted with ATTM based on the following equation⁴¹



Generated MoS_3 deposited in the support channel immediately. As to the $\text{MoS}_2\text{-I}/\text{Al}_2\text{O}_3$ catalyst, impregnated ATTM directly decomposed into MoS_3 at 280 °C in the nitrogen atmosphere according to the following equation⁴²



Both of the above-mentioned samples were calcined at 400 °C in N_2 for 4 h, and the MoS_3 precursors turned into MoS_2 active phases according to⁴³



In order to deeply investigate the formation of the pore structures, samples in different preparation stages were characterized by the nitrogen adsorption/desorption measurements.

The textural properties of the support and the catalysts were measured by nitrogen adsorption–desorption isotherms, and the results are listed in Figures 2 and S1. The isotherms are listed in Figure 2a: all samples exhibit typical IV isotherms with an H3 hysteresis loop in the relative pressure region higher than 0.5, revealing the presence of mesoporous structures according to IUPAC classification.⁴⁴ Figure 2b shows the BJH pore-size distributions for the support and catalysts. There are two types of pores that exist in the Al_2O_3 support, the serial narrow strong peaks in 4–10 nm and the broad weak peak that appears in 15–40 nm. For all the $\text{MoS}_x/\text{Al}_2\text{O}_3$ catalysts, only the narrow strong peaks are reserved, indicating that the active phase of ATTM can be scattered inside the pores of the Al_2O_3 support, no matter which method is used.

The pore structures of the Al_2O_3 support and catalysts are shown in Table 1. The specific areas and pore volumes of unsupported MoS_3 prepared by different methods are smaller

Table 1. Characteristics of the Alumina Support and Presulfided Catalysts

sample	average pore size (nm)	pore volume (cm^3/g)	BET surface area (m^2/g)
Al_2O_3	10.6	0.85	320.5
$\text{MoS}_2\text{-ID}$	3.0	0.10	37.1
$\text{MoS}_3\text{-ID}$	3.8	0.06	18.6
$\text{MoS}_2\text{-I}$		0.02	31.0
$\text{MoS}_3\text{-I}$	4.2	0.01	4.3
$\text{MoS}_3\text{-ID}/\text{Al}_2\text{O}_3$	9.1	0.68	298.5
$\text{MoS}_2\text{-ID}/\text{Al}_2\text{O}_3$	9.2	0.73	319.9
$\text{MoS}_3\text{-I}/\text{Al}_2\text{O}_3$	8.7	0.55	252.5
$\text{MoS}_2\text{-I}/\text{Al}_2\text{O}_3$	8.6	0.59	269.4

than those of as-synthesized MoS_2 , indicating that the calcination of MoS_3 under N_2 at $400\text{ }^\circ\text{C}$ can change the pore structures to a certain extent. The surface areas of unsupported MoS_2 prepared by different methods are almost the same, but the pore volume of MoS_2 -ID is 5 times as big as that of MoS_2 -I. This indicates that the depositing–calcinating process can endow MoS_2 particles with better pore structures. The average pore size, surface area, and pore volume of Al_2O_3 supports decreased after the loading of Mo. However, compared to the impregnation method, the impregnation–deposition method creates more surface areas and pore volumes for the $\text{MoS}_3/\text{Al}_2\text{O}_3$ precursors. A narrow peak appearing at 6 nm is observed in MoS_3 -ID/ Al_2O_3 (Figure 2b), indicating that new mesopores are created during the depositing process. For both catalysts, more mesopores are created after calcination at higher temperatures due to the release of S and the sintering of amorphous MoS_3 . It is noteworthy that the surface area of MoS_2 -ID/ Al_2O_3 is almost the same as that of Al_2O_3 because the porous structure of MoS_2 is reserved after deposition.

Compared to the conventional impregnation method, the impregnation–deposition method leads to about a $50\text{ m}^2/\text{g}$ increase in the specific surface area (Table 1). This may be induced by the addition of the acid and, what is more, the formation of MoS_3 particles. Contreras and co-workers⁴⁵ put forward that the acidification of ATTM could endow the material with a large surface area in the presence of polyvinylpyrrolidone. In this experiment, although no template was added, the aggregation of MoS_3 particles was inhibited by the pore structures of Al_2O_3 . Consequently, smaller MoS_3 particles were generated inside the support (as shown in Figure S2) and provided certain surface areas. After calcination in the N_2 atmosphere at $400\text{ }^\circ\text{C}$, MoS_3 decomposed into MoS_2 , and more pores were created due to the loss of S. Hence, the surface area of the catalyst became even larger.

3.3. Morphological Characterizations. It is widely accepted that the morphology of MoS_2 particles has a significant influence on the catalytic performance of Mo-based HDS catalysts.^{46,47} Therefore, representative high-resolution TEM (HRTEM) micrographs of MoS_2 -ID/ Al_2O_3 and MoS_2 -I/ Al_2O_3 catalysts were characterized, and the results are shown in Figure 3. The black thread-like fringes (with an

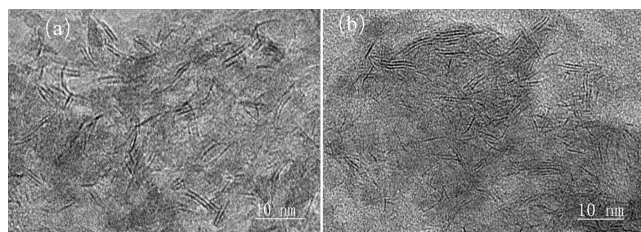


Figure 3. HRTEM images of presulfided catalysts synthesized by the impregnation method (a) MoS_2 -I/ Al_2O_3 and the impregnation–deposition method (b) MoS_2 -ID/ Al_2O_3 .

interlayer spacing of 0.62 nm) corresponding to MoS_2 slabs are well dispersed on the surface of both catalysts. In order to evaluate the influence of preparation methods on the morphology and dispersion of the MoS_2 slabs, statistical processing was performed on TEM images. The slab length and stacking number distributions for both catalysts are shown in Figure 4. The average slab length (\bar{L}_A) and average stacking

number (\bar{N}_A) of MoS_2 slabs are summarized in Table 2. For both catalysts, the slab length of MoS_2 particles is mainly distributed in 2–5 nm, and the average length is concentrated at 4 nm. The stacking number of MoS_2 slabs is mainly distributed in 1–3 in MoS_2 -I/ Al_2O_3 and 2–5 in MoS_2 -ID/ Al_2O_3 . It can be seen that the catalyst obtained by the impregnation–deposition method possesses more layers in slabs, and its average stacking number N_A is higher than that of the catalyst obtained by the impregnation method, which is in accordance with the results of XRD. Hence, the deposition of ATTM could change the morphology of MoS_2 slabs.

The proportion of Mo atoms at the edge sites (f_{Mo}) is listed in Table 2. It can be seen that f_{Mo} of the MoS_2 -I/ Al_2O_3 catalyst is slightly higher than that of the MoS_2 -ID/ Al_2O_3 catalyst, indicating that the dispersion of Mo on MoS_2 -I/ Al_2O_3 is better but not overbearing. However, the activity of the catalyst MoS_2 -ID/ Al_2O_3 is higher than that of the MoS_2 -I/ Al_2O_3 catalyst. It is well accepted that the compromise between the dispersion and the stacking number of MoS_2 slabs is crucial for achieving optimal HDS activity and selectivity.⁴⁸ To form the sufficient and accessible MoS_2 active phases, a higher and suitable stacking number is more favorable.

3.4. XPS Analyses. The binding energies of Mo 3d and S 2p and the relative atomic concentration for both catalysts are listed in Table 3. The Mo/Al ratio of the catalyst MoS_2 -ID/ Al_2O_3 is slightly smaller than that of the catalyst MoS_2 -I/ Al_2O_3 , indicating that the dispersion of Mo on MoS_2 -I/ Al_2O_3 is better. Meanwhile, the S/Mo ratio of MoS_2 -ID/ Al_2O_3 is 2.04, which is smaller than the S/Mo ratio of MoS_2 -I/ Al_2O_3 , approaching the stoichiometric ratio of MoS_2 . This means that the decomposition of ATTM is more complete in the impregnation–deposition method.

Furthermore, XPS experiments allow evaluating the relative contents of Mo and S involved in different chemical phases on the surface of the catalysts. The Mo 3d and S 2p spectra for MoS_2 -I/ Al_2O_3 and MoS_2 -ID/ Al_2O_3 are presented in Figure 5: all samples were decomposed according to the reported literature,^{49,50} which detailedly discussed the decomposition of MoS_2 samples. Concerning the spectral region of Mo 3d (Figure 5a,b), the catalysts contain two different doublets and one S 2s peak, which is not taken into account in the quantification. The doublet with the higher binding energy (232.5 and 235.7 eV) is ascribed to incompletely decomposed ATTM(VI), and the doublet with the lower energy (228.4 and 231.5 eV) is attributed to MoS_2 (IV). In order to investigate the presence of sulfur in the catalysts, the S 2p envelopes (Figure 5c,d) are decomposed into two doublets, which contain a main peak (S $2p_{3/2}$) and an associated peak (S $2p_{1/2}$). The S $2p_{3/2}$ peak at higher energy (162.6 eV) is attributed to S_2^{2-} , which often abundantly exists in MoS_3 or slightly at the edge of MoS_2 slabs.^{51,52} The one at lower binding energy (161.4 eV) is attributed to S^{2-} (MoS_2).

The relative contents of different Mo and S species are listed in Table 4. The ratio of $\text{Mo}^{4+}/(\text{Mo}^{4+} + \text{Mo}^{6+})$ for both samples is around 95%, showing that most Mo atoms in $(\text{NH}_4)_2\text{MoS}_4$ have turned into MoS_2 , whether in the impregnation–deposition method or in the impregnation method. The atom percentage of S_2^{2-} in MoS_2 -I/ Al_2O_3 is twice that in MoS_2 -ID/ Al_2O_3 , indicating that more MoS_2 active slabs are created by the impregnation–deposition method, which is in accordance with the S/Mo ratios given in Table 3. This could be attributed to the different structural compositions of MoS_3 prepared by different methods. Known as an amorphous

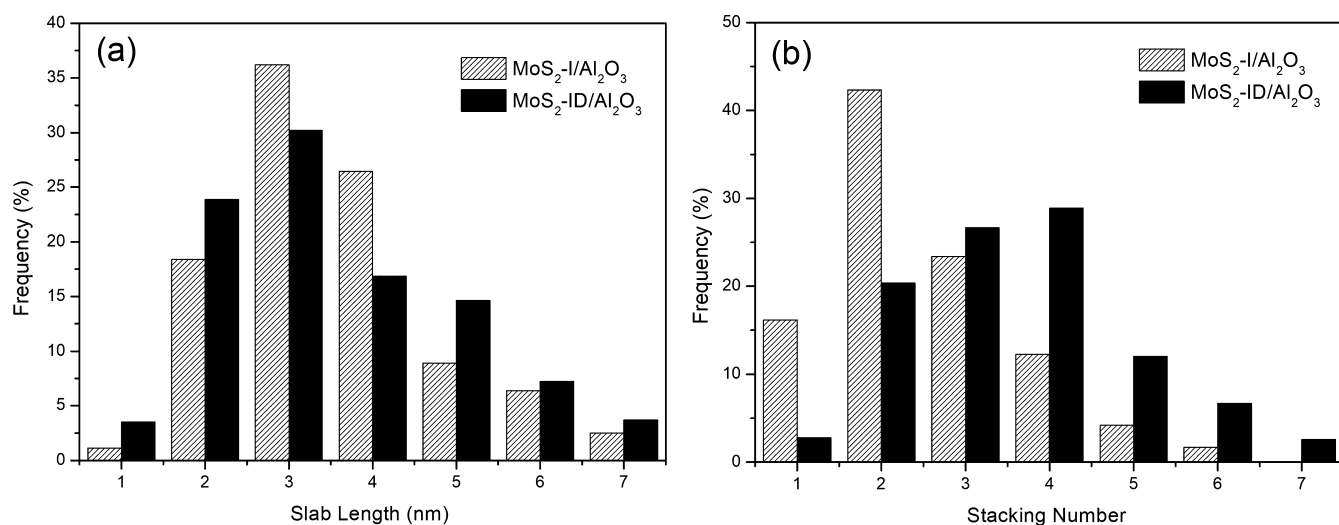


Figure 4. (a) Slab length and (b) stacking number distribution of presulfided catalysts synthesized by the impregnation method MoS₂-I/Al₂O₃ and the impregnation–deposition method MoS₂-ID/Al₂O₃.

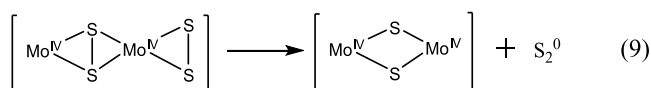
Table 2. Characteristics of the Morphology of the Presulfided Catalysts Synthesized by Different Methods

sample	average stacking number N_A	average slab length L_A (nm)	f_{Mo}
MoS ₂ -I/Al ₂ O ₃	2.02	4.06	0.28
MoS ₂ -ID/Al ₂ O ₃	3.13	4.07	0.26

Table 3. Binding Energies and Atomic Ratios Determined by XPS Experiments

sample	MoS ₂ -I/Al ₂ O ₃	MoS ₂ -ID/Al ₂ O ₃
Mo 3d _{5/2} (eV)	228.4	228.6
S 2p (eV)	161.4	161.4
Al 2p (eV)	74.3	74.2
C 1s (eV)	284.6	284.7
Atomic ratios		
Mo/Al	0.07	0.06
S/Mo	2.26	2.04

compound,⁵³ the structural formula of MoS₃ is Mo^{VI}(S²⁻)₂(S₂²⁻), which will turn into MoS₂ after calcination at 400 °C in N₂ (eq 8). The reductive removal of S₂²⁻ ligands is based on the following equation



After the loss of one S per Mo^{VI} center, reactive {Mo₃S₆} units may be preserved in each layer and aggregate to build up the MoS₂ lattice.⁵⁴ In this work, the easier formation and better pore structures of MoS₃ prepared by the impregnation–deposition method would lead to the easier reductive removal of S₂²⁻ ligands and finally create more MoS₂ active slabs.

3.5. TPR and CO-FTIR Analyses. The TPR measurement has been commonly used to characterize the active sulfur species of the MoS₂-based catalysts.⁵⁵ Figure 6 illustrates the TPR profiles of the catalysts prepared by the impregnation and the impregnation–deposition method. Two peaks appear in the range of 200–300 and 400–600 °C for both catalysts. The low-temperature peak originates from the reduction of the nonstoichiometric sulfur atoms (S_x) weakly adsorbed on

coordinated unsaturated sites (CUSs),⁵⁶ which are believed to be the catalytic active sites of MoS₂ slabs.⁵⁷ The signal of the high-temperature peak is attributed to the partial reduction of the MoS₂ crystal.^{58,59} A 65 °C downward shift in the reduction temperature for the first peak is observed in Figure 6. According to Afanasiev et al.,⁵⁶ the position of the low-temperature peak is related to the strength of the metal–sulfur bond on the MoS₂-based catalysts. In this work, when the Mo–S bonds became weaker, H₂ interacted more easily with S_x in the reduction process and finally led to the easier formation of a CUS. Besides, the areas of the low-temperature peaks allow the determination of the total number of active sites.¹¹ An enhancement of the low-temperature peak areas is also observed from the picture insert in Figure 6, indicating that more active sites will be created on MoS₂-ID/Al₂O₃ after activation in H₂ at 400 °C. Hence, the impregnation–deposition method is more beneficial for the formation of active sites compared to the impregnation method.

As a proven technique, IR spectroscopy obtained after CO adsorption (IR/CO) has been intensively used to probe the edges sites of MoS₂ slabs on MoS₂-based catalysts.⁶⁰ The IR/CO spectra of the catalysts MoS₂-ID/Al₂O₃ and MoS₂-I/Al₂O₃ are presented in Figure 7. Three bands appear at 2183, 2126, and 2055 cm⁻¹ for both catalysts. The band at 2183 cm⁻¹ can be attributed to the coordination of CO on the CUS Al³⁺ sites of the Al₂O₃ support.⁶¹ The bands at 2126 and 2055 cm⁻¹ are due to CO adsorbed on the different active sites of the MoS₂ phase. The former adsorption takes place at the Mo-edge sites of MoS₂ particles (six-coordinated Mo atoms with 50% S-coverage), while the latter takes place at the S-edge sites (100% S-coverage).⁶²

As the amount of CO adsorption can provide information on the number of active sites,⁶³ the relative areas of the peaks at 2126 and 2055 cm⁻¹ for both catalysts can be used to reveal the structure–activity relationships. The total band area of the peaks 2126 and 2055 cm⁻¹ in the catalyst MoS₂-ID/Al₂O₃ is larger than that of the catalyst MoS₂-I/Al₂O₃, which correlates nicely with TPR results, indicating that more active sites exist in this catalyst. This could be related to the easier formation of CUSs, which is caused by the weaker Mo–S bonds in the catalyst MoS₂-ID/Al₂O₃. Moreover, the appearance of 2055 cm⁻¹ in MoS₂-ID/Al₂O₃ indicates that the impregnating–

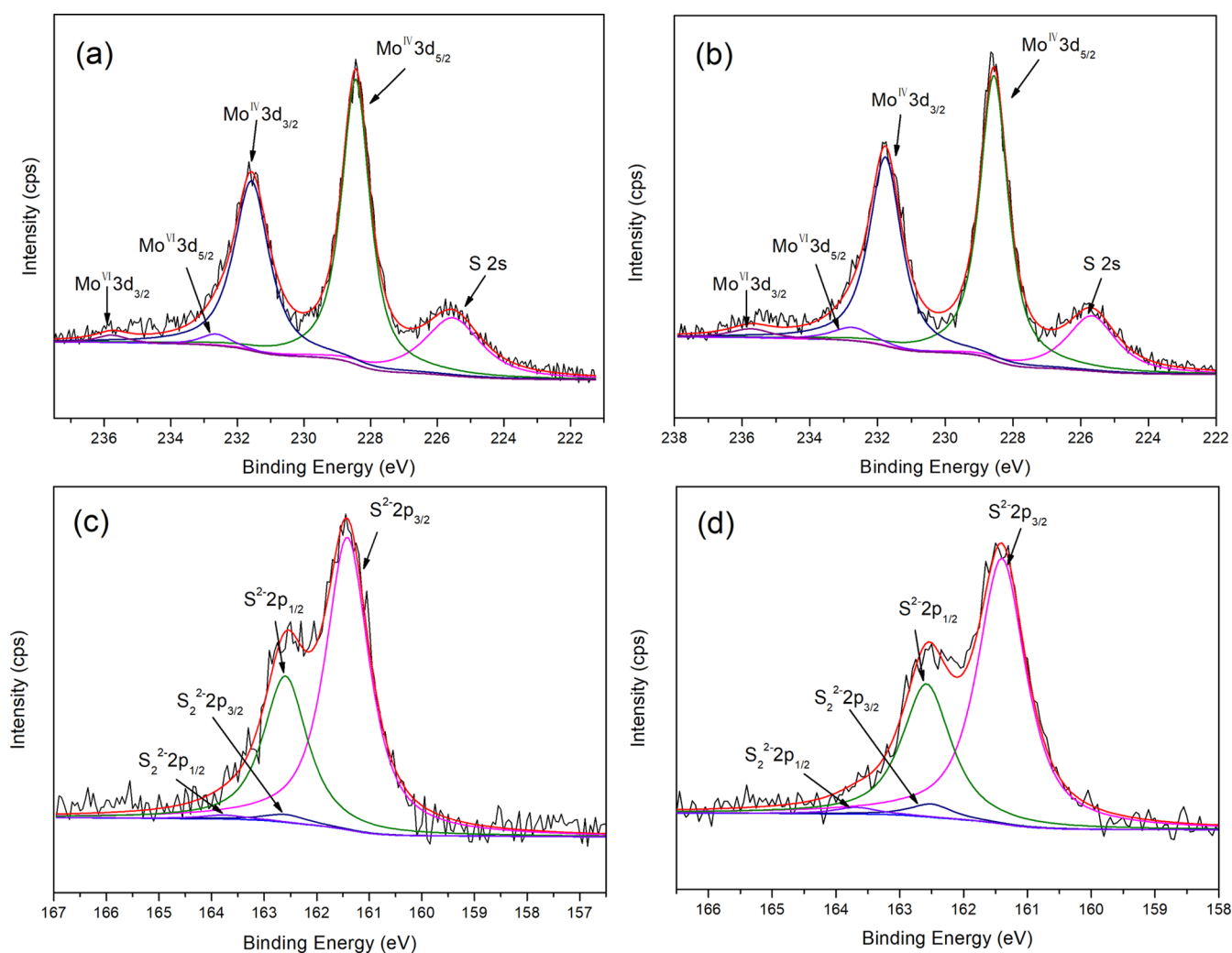


Figure 5. Mo 3d and S 2p photoelectron spectra of the catalysts synthesized by different methods: (a) Mo 3d-MoS₂-ID/Al₂O₃, (b) Mo 3d-MoS₂-I/Al₂O₃, (c) S 2p-MoS₂-ID/Al₂O₃, and (d) S 2p-MoS₂-I/Al₂O₃.

Table 4. XPS Parameters of the Different Contributions of Mo 3d_{5/2} and S 2p_{3/2} Obtained from the Catalysts

catalysts	Mo ⁶⁺		Mo ⁴⁺		S ²⁻		S ₂ ²⁻	
	BE (eV)	% at.	BE (eV)	% at.	BE (eV)	% at.	BE (eV)	% at.
MoS ₂ -ID/Al ₂ O ₃	232.6	4.5	228.4	95.5	161.4	96.5	162.6	3.5
MoS ₂ -I/Al ₂ O ₃	232.7	5.2	228.6	94.8	161.4	92.6	162.5	7.4

depositing process is more favorable for the formation of S-edge sites in the MoS₂ slabs. It is well accepted that the sulfur vacancies at different edges of MoS₂ slabs have a great influence on the reaction routes of HDS. Zheng et al.⁶⁴ considered that Mo edges were more beneficial for the direct desulfurization (DDS) pathway, while the hydrogenation (HYD) route mainly proceeded at the S-edges. In consequence, the catalyst prepared by the impregnation–deposition method might possess a higher activity and HYD selectivity than the catalyst synthesized by the impregnation method.

3.6. Catalytic Activity Assessments. DBT is a typical sulfur-containing compound in petroleum refining products and is always used to study the catalytic performance of the HDS catalyst.⁶⁵ It is well known that the HDS of DBT occurs by two parallel pathways^{66–68} (Figure S3). The first route is DDS, and its main product is biphenyl (BP), which is obtained

via the σ -adsorption of DBT and the following cleavage of the C–S bond. The second route is HYD to form cyclohexylbenzene (CHB) and bicyclohexane (BCH). In this route, DBT is first hydrogenated via the π -adsorption of the aromatic rings, producing the intermediates 1,2,3,4-tetrahydrodibenzothiophene (THDBT) and hexahydrodibenzothiophene (HHDBT). The next step involves the cleavage of the C–S bond, which yields CHB and BCH.⁶⁹ The catalytic selectivity, therefore, is expressed by the ratio between the HYD route and DDS route in the following equation

$$\frac{S_{\text{HYD}}}{S_{\text{DDS}}} = \frac{(\text{BCH} + \text{CHB} + \text{HH-DBT} + \text{TH-DBT})}{\text{BP}}$$

The HDS reaction results of DBT over the sulfided catalysts synthesized by the impregnation–deposition and impregnation method are listed in Table 5. The reaction rate of MoS₂-ID/

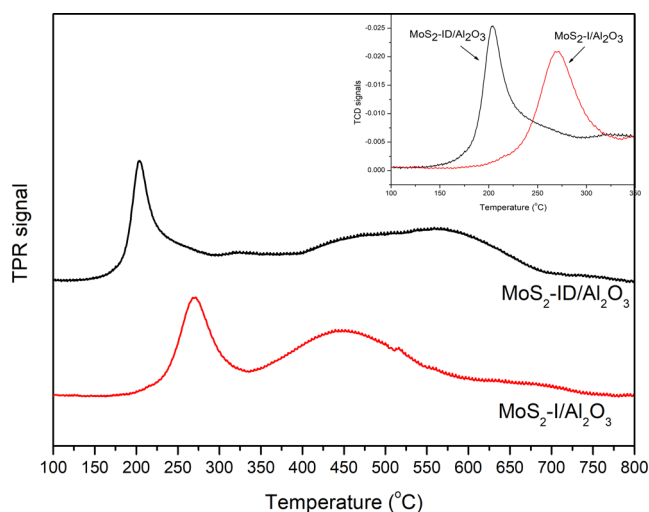


Figure 6. TPR profiles of the sulfided catalysts synthesized by the impregnation–deposition method $\text{MoS}_2\text{-ID}/\text{Al}_2\text{O}_3$ and the impregnation method $\text{MoS}_2\text{-I}/\text{Al}_2\text{O}_3$.

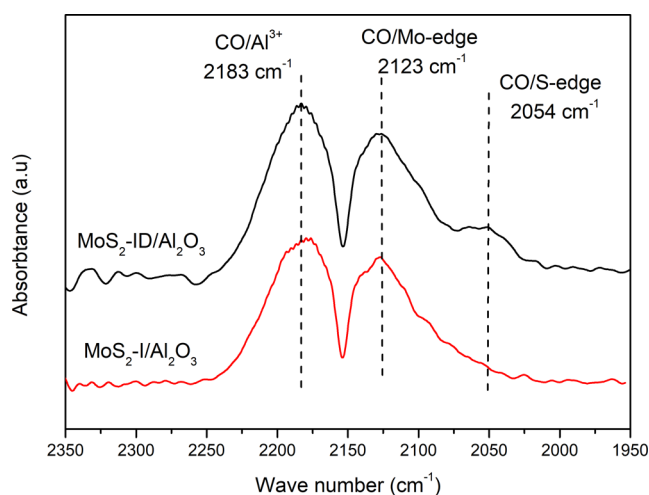


Figure 7. IR spectra of CO adsorbed ($T = 100\text{ K}$) on sulfided catalysts synthesized by the impregnation–deposition method $\text{MoS}_2\text{-ID}/\text{Al}_2\text{O}_3$ and by the impregnation method $\text{MoS}_2\text{-I}/\text{Al}_2\text{O}_3$.

Al_2O_3 ($4.5 \times 10^{-8}\text{ mol/g}\cdot\text{s}$) is 1.3 times as high as that of the catalyst $\text{MoS}_2\text{-I}/\text{Al}_2\text{O}_3$ ($3.4 \times 10^{-8}\text{ mol/g}\cdot\text{s}$). This indicates that more DBT reacted on $\text{MoS}_2\text{-ID}/\text{Al}_2\text{O}_3$ under the same reaction conditions. The DBT conversion is 53.2% for the catalyst $\text{MoS}_2\text{-I}/\text{Al}_2\text{O}_3$ while 70.5% for the catalyst $\text{MoS}_2\text{-ID}/\text{Al}_2\text{O}_3$. The content of BP is almost the same for both catalysts due to the similar steric hindrance effect of DBT on the DDS pathway. The higher HDS activity of the catalyst $\text{MoS}_2\text{-ID}/\text{Al}_2\text{O}_3$ can be explained by the higher amounts of active sites created during the preparation and reaction process. Compared to the impregnation method, MoS_3 was directly

deposited on the Al_2O_3 support by the precipitation process under mild conditions and could be reduced to MoS_2 more completely, as evidenced by the S/Mo ratio of XPS results (Table 3). Moreover, it appears from the TPR results (Figure 6) that for the impregnation–precipitation method, the MoS_2 particles were more easily reduced, and more active sites could be created accordingly. Furthermore, the higher amounts of active sites created by this method could also be proved by the results of CO-FTIR (Figure 7).

The ratio of HYD/DDS shows that the dominant route of HDS over the two catalysts is the hydrogenation route. Particularly, the $S_{\text{HYD}}/S_{\text{DDS}}$ ratio in the catalyst $\text{MoS}_2\text{-ID}/\text{Al}_2\text{O}_3$ is 1.5 times as large as that of the catalyst $\text{MoS}_2\text{-I}/\text{Al}_2\text{O}_3$, indicating the superior activity of the former catalyst provided by the HYD route. This can be attributed to two factors: (1) the higher average stacking number and (2) the more S-edge sites in the MoS_2 slabs of the catalyst $\text{MoS}_2\text{-ID}/\text{Al}_2\text{O}_3$. Hensen et al.⁷⁰ put forward that the HYD rate increased with an increasing stacking number of MoS_2 slabs, which would favor the less hampered planar adsorption of DBT. Besides, the S-edge sites of the MoS_2 slabs are mainly responsible for the HYD route as proved by the CO-FTIR results. Hence, more DBT turns into CHB, BCH, and TH-DBT in the catalyst prepared by the impregnation–deposition method.

4. CONCLUSIONS

In conclusion, a novel impregnation–deposition method was used to synthesize a presulfided $\text{MoS}_2/\text{Al}_2\text{O}_3$ catalyst with large surface area and excellent HDS active performance. Compared with the conventional impregnation method, the impregnation–deposition method produces catalysts with larger surface areas mainly by generating mesostructured MoS_2 particles inside the Al_2O_3 support, as proved by the N_2 adsorption–desorption analyses. The average slab length of the MoS_2 particles in both catalysts is almost the same (about 4.0 nm), but the stacking number of the MoS_2 particles is higher for the impregnation–deposition method than that of the impregnation method, as proved by the HRTEM images and XRD patterns. The formation of MoS_2 active phases is also more completed by the impregnation–deposition method based on the XPS analyses. TPR reveals that the Mo–S bonds in the catalysts become weaker when the impregnation–deposition method is used. Hence, more active sites, especially more active S-edges, are created in the as-synthesized catalyst as proved by the TPR and CO-FTIR data. The reaction rate and the HYD/DDS ratio of the DBT on the catalysts synthesized by the impregnation–deposition method are 1.3 times and 1.5 times as high as those of the impregnation method, respectively. All the results prove that the novel impregnation–deposition method not only increases the activity of the presulfided Mo catalyst but also changes the contribution of the HYD and DDS pathways.

Table 5. Distribution of HDS Reaction Products

samples	distribution (wt %)							$r_{\text{DBT}}/\times 10^{-8}\text{ mol/g}\cdot\text{s}$	$S_{\text{HYD}}/S_{\text{DDS}}^b$
	BCH	CHB	BP	HH-DBT	TH-DBT	DBT	HDS ^a /%		
$\text{MoS}_2\text{-ID}/\text{Al}_2\text{O}_3$	3.6	35.6	22.8	0.8	7.7	29.5	70.5	4.5	2.1
$\text{MoS}_2\text{-I}/\text{Al}_2\text{O}_3$	3.0	22.4	22.2	0.3	5.3	46.8	53.2	3.4	1.4

^aHDS (%) = DBT conversion (%) = TH-DBT + HH-DBT + CHB + BCH + BP. ^b $S_{\text{HYD}}/S_{\text{DDS}}$: (CHB + BCH + HH-DBT + TH-DBT)/BP.

■ ASSOCIATED CONTENT

SI Supporting Information

The Supporting Information is available free of charge at <https://pubs.acs.org/doi/10.1021/acsomega.2c07123>.

Textural properties of MoS₃, morphologies of the presulfided MoS₃/Al₂O₃ and MoS₂/Al₂O₃ catalysts, and reaction networks for the HDS of DBT (PDF)

■ AUTHOR INFORMATION

Corresponding Authors

Xuehui Li – College of Chemistry and Pharmaceutical Sciences, Qingdao Agricultural University, Qingdao 266109, China; orcid.org/0000-0003-2088-239X; Email: lixuehui@qau.edu.cn

Long Hao – College of Chemistry and Pharmaceutical Sciences, Qingdao Agricultural University, Qingdao 266109, China; orcid.org/0000-0001-5326-784X; Email: haol@qau.edu.cn

Authors

Xuefeng Wang – College of Chemistry and Pharmaceutical Sciences, Qingdao Agricultural University, Qingdao 266109, China

Jing Ning – College of Chemistry and Pharmaceutical Sciences, Qingdao Agricultural University, Qingdao 266109, China; orcid.org/0000-0001-9325-519X

Hongtao Wei – College of Chemistry and Pharmaceutical Sciences, Qingdao Agricultural University, Qingdao 266109, China; orcid.org/0000-0001-5675-9735

Complete contact information is available at: <https://pubs.acs.org/10.1021/acsomega.2c07123>

Author Contributions

[†]X.L. and X.W. contributed equally to this work.

Notes

The authors declare no competing financial interest.

■ ACKNOWLEDGMENTS

This work was supported by the Doctoral Fund of Qingdao Agriculture University (665-1120048).

■ REFERENCES

- (1) Wang, E.; Yang, F.; Song, M.; Chen, G.; Zhang, Q.; Wang, F.; Bing, L.; Wang, G.; Han, D. Recent advances in the unsupported catalysts for the hydrodesulfurization of fuel. *Fuel Process. Technol.* **2022**, *235*, 107386.
- (2) Saleh, T. A. Characterization, determination and elimination technologies for sulfur from petroleum: Toward cleaner fuel and a safe environment. *Trends Environ. Anal. Chem.* **2020**, *25*, No. e00080.
- (3) Mguni, L. L.; Yao, Y.; Liu, X.; Yuan, Z.; Hildebrandt, D. Ultra-deep desulfurization of both model and commercial diesel fuels by adsorption method. *J. Environ. Chem. Eng.* **2019**, *7*, 102957.
- (4) Leal, E.; Torres-Mancera, P.; Ancheyta, J. Catalyst stacking technology as a viable solution to ultralow sulfur diesel production. *Energy Fuels* **2022**, *36*, 3201–3218.
- (5) Weng, X.; Cao, L.; Zhang, G.; Chen, F.; Zhao, L.; Zhang, Y.; Gao, J.; Xu, C. Ultra-deep hydrodesulfurization of diesel: Mechanisms, catalyst design strategies, and challenges. *Ind. Eng. Chem. Res.* **2020**, *59*, 21261–21274.
- (6) Shafiq, I.; Shafique, S.; Akhter, P.; Yang, W.; Hussain, M. Recent developments in alumina supported hydrodesulfurization catalysts for the production of sulfur-free refinery products: A technical review. *Catal. Rev.* **2022**, *64*, 1–86.
- (7) Sharifvaghefi, S.; Yang, B.; Zheng, Y. New insights on the role of H₂S and sulfur vacancies on dibenzothiophene hydrodesulfurization over MoS₂ edges. *Appl. Catal., A* **2018**, *566*, 164–173.
- (8) Al-Attas, T. A.; Ali, S. A.; Zahir, M. H.; Xiong, Q.; Al-Bogami, S. A.; Malaibari, Z. O.; Razzak, S. A.; Hossain, M. M. Recent advances in heavy oil upgrading using dispersed catalysts. *Energy Fuels* **2019**, *33*, 7917–7949.
- (9) Saleh, T. A. Carbon nanotube-incorporated alumina as a support for MoNi catalysts for the efficient hydrodesulfurization of thiophenes. *Chem. Eng. J.* **2021**, *404*, 126987.
- (10) Ishag, A.; Sun, Y. Recent Advances in two-dimensional MoS₂ nanosheets for environmental application. *Ind. Eng. Chem. Res.* **2021**, *60*, 8007–8026.
- (11) Liu, B.; Liu, L.; Chai, Y.; Zhao, J.; Li, Y.; Liu, D.; Liu, Y.; Liu, C. Effect of sulfiding conditions on the hydrodesulfurization performance of the ex-situ presulfided CoMoS/γ-Al₂O₃ catalysts. *Fuel* **2018**, *234*, 1144–1153.
- (12) Tanimu, A.; Alhooshani, K. Advanced hydrodesulfurization catalysts: A review of design and synthesis. *Energy Fuels* **2019**, *33*, 2810–2838.
- (13) Saleh, T. A. Global trends in technologies and nanomaterials for removal of sulfur organic compounds: Clean energy and green environment. *J. Mol. Liq.* **2022**, *359*, 119340.
- (14) Hinnemann, B.; Nørskov, J. K.; Topsøe, H. A density functional study of the chemical differences between type I and type II MoS₂-based structures in hydrotreating catalysts. *J. Phys. Chem. B* **2004**, *109*, 2245–2253.
- (15) Wang, H.; Yang, F.; Yang, Z.; Yang, H.; Wu, Y. Synthesis, characterization, and hydrotreating activity of NiW presulfurized catalysts prepared via a tetrathiotungstate-intercalated NiAl LDH. *ACS Omega* **2020**, *5*, 23854–23865.
- (16) Liu, B.; Zhao, K.; Chai, Y.; Li, Y.; Liu, D.; Liu, Y.; Liu, C. Slurry phase hydrocracking of vacuum residue in the presence of presulfided oil-soluble MoS₂ catalyst. *Fuel* **2019**, *246*, 133–140.
- (17) Huirache-Acuña, R.; Alonso-Núñez, G.; Paraguay-Delgado, F.; Lara-Romero, J.; Berhault, G.; Rivera-Muñoz, E. M. Unsupported trimetallic CoMoW sulfide HDS catalysts prepared by in situ decomposition of sulfur-containing precursors. *Catal. Today* **2015**, *250*, 28–37.
- (18) Sun, K.; Guo, H.; Jiao, F.; Chai, Y.; Li, Y.; Liu, B.; Mintova, S.; Liu, C. Design of an intercalated Nano-MoS₂ hydrophobic catalyst with high rim sites to improve the hydrogenation selectivity in hydrodesulfurization reaction. *Appl. Catal., B* **2021**, *286*, 119907.
- (19) Huirache-Acuña, R.; Navarro Yerga, R. M.; Pawelec, B. Hydrodesulfurization on supported CoMoS₂ catalysts ex ammonium tetrathiomolybdate: Effects of support morphology and Al modification method. *Top. Catal.* **2022**, *65*, 1394–1407.
- (20) Hu, D.; Li, Y.; Mei, J.; Wang, G.; Xiao, C.; Liu, C.; Meng, Q.; Li, H.; Fu, S.; Duan, A. High-dispersed Ni-Mo-S active phases within hierarchical pore materials by introducing the cationic protective shell during the impregnation process for hydrodesulfurization. *Fuel* **2020**, *263*, 116701.
- (21) Sundaramurthy, V.; Dalai, A. K.; Adjaye, J. Tetraalkylthiomolybdates-derived Co(Ni)Mo/γ-Al₂O₃ sulfide catalysts for gas oil hydrotreating. *J. Mol. Catal. A: Chem.* **2008**, *294*, 20–26.
- (22) Niefind, F.; Bensch, W.; Deng, M.; Kienle, L.; Cruz-Reyes, J.; Del Valle Granados, J. M. Co-promoted MoS₂ for hydrodesulfurization: New preparation method of MoS₂ at room temperature and observation of massive differences of the selectivity depending on the activation atmosphere. *Appl. Catal., A* **2015**, *497*, 72–84.
- (23) Bezverkhyy, I.; Afanasiev, P.; Geantet, C.; Lacroix, M. Highly active (Co)MoS₂/Al₂O₃ hydrodesulfurization catalysts prepared in aqueous solution. *J. Catal.* **2001**, *204*, 495–497.
- (24) Bezverkhyy, I.; Afanasiev, P.; Lacroix, M. Promotion of highly loaded MoS₂/Al₂O₃ hydrodesulfurization catalysts prepared in aqueous solution. *J. Catal.* **2005**, *230*, 133–139.
- (25) Lee, Y. H.; Zhang, X. Q.; Zhang, W.; Chang, M. T.; Lin, C. T.; Chang, K. D.; Yu, Y. C.; Wang, J. T. W.; Chang, C. S.; Li, L. J.; Lin, T.

- W. Synthesis of large-area MoS₂ atomic layers with chemical vapor deposition. *Adv. Mater.* **2012**, *24*, 2320–2325.
- (26) Vattikuti, S. V. P.; Byon, C.; Reddy, C. V. Synthesis of MoS₂ multi-wall nanotubes using wet chemical method with H₂O₂ as growth promoter. *Superlattices Microstruct.* **2015**, *85*, 124–132.
- (27) Serna, M. I.; Yoo, S. H.; Moreno, S.; Xi, Y.; Oviedo, J. P.; Choi, H.; Alshareef, H. N.; Kim, M. J.; Minary-Jolandan, M.; Quevedo-Lopez, M. A. Large-area deposition of MoS₂ by pulsed laser deposition with in situ thickness control. *ACS Nano* **2016**, *10*, 6054–6061.
- (28) Li, M.; Yao, J.; Wu, X.; Zhang, S.; Xing, B.; Niu, X.; Yan, X.; Yu, Y.; Liu, Y.; Wang, Y. P-type doping in large-area monolayer MoS₂ by chemical vapor deposition. *ACS Appl. Mater. Interfaces* **2020**, *12*, 6276–6282.
- (29) Arshad, F.; Aubry, C.; Zou, L. Highly permeable MoS₂ nanosheet porous membrane for organic matter removal. *ACS Omega* **2022**, *7*, 2419–2428.
- (30) Hu, X.; Lu, S.; Tian, J.; Wei, N.; Song, X.; Wang, X.; Cui, H. The selective deposition of MoS₂ nanosheets onto (101) facets of TiO₂ nanosheets with exposed (001) facets and their enhanced photocatalytic H₂ production. *Appl. Catal., B* **2019**, *241*, 329–337.
- (31) Zafropoulou, I.; Katsiotis, M. S.; Boukos, N.; Karakassides, M. A.; Stephen, S.; Tzitzios, V.; Fardis, M.; Vlades, R. V.; Alhassan, S. M.; Papavassiliou, G. In situ deposition and characterization of MoS₂ nanolayers on carbon nanofibers and nanotubes. *J. Phys. Chem. C* **2013**, *117*, 10135–10142.
- (32) Joyner, J.; Oliveira, E. F.; Yamaguchi, H.; Kato, K.; Vinod, S.; Galvao, D. S.; Salpekar, D.; Roy, S.; Martinez, U.; Tiwary, C. S.; Ozden, S.; Ajayan, P. M. Graphene supported MoS₂ structures with high defect density for an efficient HER electrocatalysts. *ACS Appl. Mater. Interfaces* **2020**, *12*, 12629–12638.
- (33) Shi, G.; Han, W.; Yuan, P.; Fan, Y.; Bao, X. Sulfided Mo/Al₂O₃ hydrodesulfurization catalyst prepared by ethanol-assisted chemical deposition method. *Chin. J. Catal.* **2013**, *34*, 659–666.
- (34) Gao, Y.; Han, W.; Long, X.; Nie, H.; Li, D. Preparation of hydrodesulfurization catalysts using MoS₃ nanoparticles as a precursor. *Appl. Catal., B* **2018**, *224*, 330–340.
- (35) Alonso, G.; Siadati, M. H.; Berhault, G.; Aguilar, A.; Fuentes, S.; Chianelli, R. R. Synthesis of tetraalkylammonium thiometalate precursors and their concurrent in situ activation during hydrodesulfurization of dibenzothiophene. *Appl. Catal., A* **2004**, *263*, 109–117.
- (36) Li, X.; Chai, Y.; Liu, B.; Liu, H.; Li, J.; Zhao, R.; Liu, C. Hydrodesulfurization of 4,6-dimethyldibenzothiophene over CoMo catalysts supported on γ -alumina with different morphology. *Ind. Eng. Chem. Res.* **2014**, *53*, 9665–9673.
- (37) López-Benítez, A.; Berhault, G.; Guevara-Lara, A. NiMo catalysts supported on Mn-Al₂O₃ for dibenzothiophene hydrodesulfurization application. *Appl. Catal., B* **2017**, *213*, 28–41.
- (38) Zhou, W.; Liu, M.; Zhang, Q.; Wei, Q.; Ding, S.; Zhou, Y. Synthesis of NiMo catalysts supported on gallium-containing mesoporous Y zeolites with different gallium contents and their high activities in the hydrodesulfurization of 4,6-dimethyldibenzothiophene. *ACS Catal.* **2017**, *7*, 7665–7679.
- (39) Liu, H.; Liu, C.; Yin, C.; Chai, Y.; Li, Y.; Liu, D.; Liu, B.; Li, X.; Wang, Y.; Li, X. Preparation of highly active unsupported nickel–zinc–molybdenum catalysts for the hydrodesulfurization of dibenzothiophene. *Appl. Catal., B* **2015**, *174–175*, 264–276.
- (40) Pakharukova, V. P.; Yatsenko, D. A.; Gerasimov, E. Y.; Vlasova, E.; Bukhtiyarova, G. A.; Tsybulya, S. V. Total scattering debye function analysis: Effective approach for structural studies of supported MoS₂-based hydrotreating catalysts. *Ind. Eng. Chem. Res.* **2020**, *59*, 10914–10922.
- (41) Guzmán, H. J.; Vitale, G.; Carbognani-Ortega, L.; Scott, C. E.; Pereira-Almao, P. Molybdenum sulfide nanoparticles prepared using starch as capping agent. Redispersion and activity in Athabasca Bitumen hydrotreating. *Catal. Today* **2021**, *377*, 38–49.
- (42) Nath, M.; Govindaraj, A.; Rao, C. N. R. Simple synthesis of MoS₂ and WS₂ nanotubes. *Adv. Mater.* **2001**, *13*, 283–286.
- (43) Chen, J.; Zhang, C.; Huang, M.; Zhang, J.; Zhang, J.; Liu, H.; Wang, G.; Wang, R. The activation of porous atomic layered MoS₂ basal-plane to induce adjacent Mo atom pairs promoting high efficiency electrochemical N₂ fixation. *Appl. Catal., B* **2021**, *285*, 119810.
- (44) Ali, I.; Al-Arfaj, A. A.; Saleh, T. A. Carbon nanofiber-doped zeolite as support for molybdenum based catalysts for enhanced hydrodesulfurization of dibenzothiophene. *J. Mol. Liq.* **2020**, *304*, 112376.
- (45) Contreras, C.; Isquierdo, F.; Pereira-Almao, P.; Scott, C. E. Effect of particle size on the HDS activity of molybdenum sulfide. *J. Nanotechnol.* **2016**, *2016*, 3752484.
- (46) Zhang, C.; Li, P.; Liu, X.; Liu, T.; Jiang, Z.; Li, C. Morphology-performance relation of (Co)MoS₂ catalysts in the hydrodesulfurization of FCC gasoline. *Appl. Catal., A* **2018**, *556*, 20–28.
- (47) Niu, X.; Zhou, W.; Han, Y.; Liu, Y. Controllable synthesis of defect-rich CoMoS catalysts with different morphologies for the ultradeep hydrodesulfurization of 4,6-dimethyldibenzothiophene. *Langmuir* **2021**, *37*, 14254–14264.
- (48) Fan, Y.; Shi, G.; Liu, H.; Bao, X. Morphology tuning of supported MoS₂ slabs for selectivity enhancement of fluid catalytic cracking gasoline hydrodesulfurization catalysts. *Appl. Catal., B* **2009**, *91*, 73–82.
- (49) Ninh, T. K. T.; Massin, L.; Laurenti, D.; Vrinat, M. A new approach in the evaluation of the support effect for NiMo hydrodesulfurization catalysts. *Appl. Catal., A* **2011**, *407*, 29–39.
- (50) Bravo-Sanchez, M.; Romero-Galarza, A.; Ramírez, J.; Gutiérrez-Alejandre, A.; Solís-Casados, D. A. Quantification of the sulfidation extent of Mo in CoMo HDS catalyst through XPS. *Appl. Surf. Sci.* **2019**, *493*, 587–592.
- (51) Iranmahboob, J.; Gardner, S. D.; Toghiani, H.; Hill, D. O. XPS study of molybdenum sulfide catalyst exposed to CO and H₂. *J. Colloid Interface Sci.* **2004**, *270*, 123–126.
- (52) Wang, D.; Wang, L.; Jiao, Y.; Wu, A.; Yan, H.; Kang, X.; Tian, C.; Liu, J.; Fu, H. The confined growth of few-layered and ultrashort-slab Ni-promoted MoS₂ on reduced graphene oxide for deep-degree hydrodesulfurization. *Nano Res.* **2022**, *15*, 7052–7062.
- (53) Hibble, S. J.; Wood, G. B. Modeling the structure of amorphous MoS₃: A neutron diffraction and reverse monte carlo study. *J. Am. Chem. Soc.* **2004**, *126*, 959–965.
- (54) Weber, T.; Muijsers, J. C.; Niemantsverdriet, J. W. Structure of amorphous MoS₃. *J. Phys. Chem.* **1995**, *99*, 9194–9200.
- (55) Lu, J.; Fang, J.; Xu, Z.; He, D.; Feng, S.; Li, Y.; Wan, G.; He, S.; Wu, H.; Luo, Y. Facile synthesis of few-layer and ordered K-promoted MoS₂ nanosheets supported on SBA-15 and their potential application for heterogeneous catalysis. *J. Catal.* **2020**, *385*, 107–119.
- (56) Afanasiev, P. On the interpretation of temperature programmed reduction patterns of transition metals sulphides. *Appl. Catal., A* **2006**, *303*, 110–115.
- (57) Zheng, P.; Xiao, C.; Cao, Z.; Shi, Y.; Wang, G.; Duan, A.; Xu, C. DFT insights into the hydrodesulfurization mechanisms of different sulfur-containing compounds over CoMoS active phase: Effect of the brim and CUS sites. *Chem. Eng. Sci.* **2021**, *231*, 116311.
- (58) Yoosuk, B.; Kim, J. H.; Song, C.; Ngamcharussrivichai, C.; Prasassarakich, P. Highly active MoS₂, CoMoS₂ and NiMoS₂ unsupported catalysts prepared by hydrothermal synthesis for hydrodesulfurization of 4,6-dimethyldibenzothiophene. *Catal. Today* **2008**, *130*, 14–23.
- (59) Baubet, B.; Devers, E.; Hugon, A.; Leclerc, E.; Afanasiev, P. The influence of MoS₂ slab 2D morphology and edge state on the properties of alumina-supported molybdenum sulfide catalysts. *Appl. Catal., A* **2014**, *487*, 72–81.
- (60) Chen, J.; Labruyere, V.; Maugé, F.; Quoineaud, A.-A.; Hugon, A.; Oliviero, L. IR spectroscopic evidence for MoS₂ morphology change with sulfidation temperature on MoS₂/Al₂O₃ Catalyst. *J. Phys. Chem. C* **2014**, *118*, 30039–30044.
- (61) Chen, J.; Dominguez Garcia, E.; Oliviero, L.; Maugé, F. How the CO molar extinction coefficient influences the quantification of active sites from CO adsorption followed by IR spectroscopy? A case

study on MoS₂/Al₂O₃ catalysts prepared with citric acid. *J. Catal.* **2015**, *332*, 77–82.

(62) Oliviero, L.; Travert, A.; Dominguez Garcia, E.; Chen, J.; Maugé, F. Catalysis by sulfides: Advanced IR/CO spectroscopy for the identification of the most active sites in hydrodesulfurization reactions. *J. Catal.* **2021**, *403*, 87–97.

(63) Liu, B.; Chai, Y.; Wang, Y.; Zhang, T.; Liu, Y.; Liu, C. A simple technique for preparation of presulfided eggshell MoS₂/Al₂O₃ catalysts and kinetics approach for highly selective hydrodesulfurization of FCC gasoline. *Appl. Catal., A* **2010**, *388*, 248–255.

(64) Zheng, P.; Duan, A.; Chi, K.; Zhao, L.; Zhang, C.; Xu, C.; Zhao, Z.; Song, W.; Wang, X.; Fan, J. Influence of sulfur vacancy on thiophene hydrodesulfurization mechanism at different MoS₂ edges: A DFT study. *Chem. Eng. Sci.* **2017**, *164*, 292–306.

(65) Saleh, T. A. Simultaneous adsorptive desulfurization of diesel fuel over bimetallic nanoparticles loaded on activated carbon. *J. Cleaner Prod.* **2018**, *172*, 2123–2132.

(66) Vanrysselberghe, V.; Froment, G. F. Hydrodesulfurization of dibenzothiophene on a CoMo/Al₂O₃ catalyst: Reaction network and kinetics. *Ind. Eng. Chem. Res.* **1996**, *35*, 3311–3318.

(67) Egorova, M.; Prins, R. Hydrodesulfurization of dibenzothiophene and 4,6-dimethyldibenzothiophene over sulfided NiMo/ γ -Al₂O₃, CoMo/ γ -Al₂O₃, and Mo/ γ -Al₂O₃ catalysts. *J. Catal.* **2004**, *225*, 417–427.

(68) Bataille, F.; Lemberon, J.-L.; Michaud, P.; Pérot, G.; Vrinat, M.; Lemaire, M.; Schulz, E.; Breysse, M.; Kasztelan, S. Alkyldibenzothiophenes hydrodesulfurization-promoter effect, reactivity, and reaction mechanism. *J. Catal.* **2000**, *191*, 409–422.

(69) Saleh, T. A.; Sulaiman, K. O.; AL-Hammadi, S. A. Effect of carbon on the hydrodesulfurization activity of MoCo catalysts supported on zeolite/ active carbon hybrid supports. *Appl. Catal., B* **2020**, *263*, 117661.

(70) Hensen, E. J. M.; Kooyman, P. J.; van der Meer, Y.; van der Kraan, A. M.; de Beer, V. H. J.; van Veen, J. A. R.; van Santen, R. A. The relation between morphology and hydrotreating activity for supported MoS₂ particles. *J. Catal.* **2001**, *199*, 224–235.